Biomaterials 35 (2014) 8467–8478

Contents lists available at ScienceDirect

Biomaterials

journal homepage: www.elsevier.com/locate/biomaterials

Endocytosis of PEGylated nanoparticles accompanied by structural and free energy changes of the grafted polyethylene glycol

Ying Li [a], Martin Kröger [b], Wing Kam Liu [a, c, *]

[a] Department of Mechanical Engineering, Northwestern University, 2145 Sheridan Road, Evanston, IL 60208-0311, USA
[b] Department of Materials, Polymer Physics, ETH Zurich, CH-8093 Zurich, Switzerland
[c] Distinguished Scientists Program Committee at King Abdulaziz University (KAU), Jeddah, Saudi Arabia

ARTICLE INFO

Article history:
Received 6 June 2014
Accepted 17 June 2014
Available online 4 July 2014

Keywords:
PEGylated NP
Cell membrane
Particle internalization
Surface grafting
Drug delivery

ABSTRACT

Nanoparticles (NPs) are in use to efficiently deliver drug molecules into diseased cells. The surfaces of NPs are usually grafted with polyethylene glycol (PEG) polymers, during so-called PEGylation, to improve water solubility, avoid aggregation, and prevent opsonization during blood circulation. The interplay between grafting density σ_p and grafted PEG polymerization degree N makes cellular uptake of PEGylated NPs distinct from that of bare NPs. To understand the role played by grafted PEG polymers, we study the endocytosis of 8 nm sized PEGylated NPs with different σ_p and N through large scale dissipative particle dynamics (DPD) simulations. The free energy change $F_{polymer}$ of grafted PEG polymers, before and after endocytosis, is identified to have an effect which is comparable to, or even larger than, the bending energy of the membrane during endocytosis. Based on self-consistent field theory $F_{polymer}$ is found to be dependent on both σ_p and N. By incorporating $F_{polymer}$, the critical ligand-receptor binding strength for PEGylated NPs to be internalized can be correctly predicted by a simple analytical equation. Without considering $F_{polymer}$, it turns out impossible to predict whether the PEGylated NPs will be delivered into the diseased cells. These simulation results and theoretical analysis not only provide new insights into the endocytosis process of PEGylated NPs, but also shed light on the underlying physical mechanisms, which can be utilized for designing efficient PEGylated NP-based therapeutic carriers with improved cellular targeting and uptake.

1. Introduction

Nanoparticles (NPs) have demonstrated promising properties as therapeutic carriers which can efficiently deliver drug molecules into diseased cells to treat numerous physiological disorders [1,2]. In the NP-mediated drug delivery process, one of the most important steps is the internalization of NPs, called 'endocytosis' [3–7]. Endocytosis is an energetically driven process by which the NPs are enveloped by the lipid bilayer of the cell membrane. Cells import and export selected extracellular molecules, as well as NPs, through endocytosis and exocytosis, respectively. Depending on the cell type, the internalization mechanism and the properties of the NPs, the endocytosis process can involve a few different pathways: phagocytosis, pinocytosis, and clathrin-dependent and independent receptor-mediated endocytosis [3,4,6]. Among them, receptor-mediated endocytosis is the most efficient pathway for cellular uptake of NPs. In this process, the surfaces of NPs are coated by ligands that recognize and bind to the cell-surface receptors. If the particle is too small, the ligand-receptor binding strength is too weak to overcome the energy barrier created by bending of the cell membrane [8,9], and the NP cannot be fully internalized. On the other hand, when the particle is too large, the cellular uptake of NPs is prohibited as the receptors expressed over the cell membrane have to diffuse to the site of NP invagination [8]. Therefore, endocytosis may not occur at all or may possibly develop over a long time period, limited by the diffusivity of receptors [8,10]. Experimental studies reveal that the optimal NP diameter for receptor-mediated endocytosis is about 25–50 nm [11,12], which agrees well with theoretical predictions [8–10,13,14] and computer simulations [15–17]. Subsequently, the shape, surface charge, and stiffness of NPs were found to play specific roles in endocytosis [3–6,18–22].

In the design of the first-generation (i.e. non-PEGylated) NPs, particles with different sizes, shapes and surface charges were

* Corresponding author. Department of Mechanical Engineering, Northwestern University, 2145 Sheridan Road, Evanston, IL 60208-0311, USA. Tel.: +1 847 491 7094; fax: +1 847 491 3915.
E-mail address: w-liu@northwestern.edu (W.K. Liu).

http://dx.doi.org/10.1016/j.biomaterials.2014.06.032

synthesized. These features offer extra degrees of freedom over the freely administrated drug molecules for potentially improving their accumulation at the diseased sites; the importance of NP size and surface charge has been well established through experiments [11,12,23]. However, most of these experimental studies operated with serum-free media or did not consider the serum-protein interactions with NPs. In vivo data show that these first-generation NPs are rapidly cleared after injection [24]. Moreover, the NPs are unstable and usually internalized by the immune cells (macrophages) during circulation. To overcome these problems, surfaces of second-generation NPs were grafted with polymer such as polyethylene glycol (PEG), which is known to be hydrophilic and biocompatible. With the help of PEGylation, the second-generation NPs demonstrated improved stability and targeting in biological systems. At the same time, the properties of these NPs were dramatically different. Due to the PEG-mediated shielding of the NP surface charge PEGylated NPs can be well dispersed in solution. More importantly, a 'stealth' shell is formed by the grafted PEG polymer that tends to prevent clearance by the immune system (opsonization) [25]. PEGylated NPs therefore display prolonged blood circulation time. Furthermore, the cellular uptake of PEGylated NPs can be reduced due to the steric interactions between grafted chains and the cell membrane [19].

To improve the endocytosis of PEGylated NPs, all the free ends of grafted PEG polymers are typically conjugated with targeting moieties such as cell-penetrating peptides (CPPs) [26–28], arginylglycylaspartic acid (RGD) peptides [29,30], or anti-HER2 antibodies [19]. With the help of these specific ligand-receptor interactions, the cellular uptake of PEGylated NPs is tremendously enhanced. Like their ungrafted counterparts, PEGylated NPs display size-dependent endocytosis, but the size dependence is more complex. Oh et al. found that PEGylated gold (Au) NPs with $d = 2.4$ nm core diameters can be delivered into the nucleus, while NPs with $d = 5.5$ nm and $d = 8.2$ nm can only be partially delivered into the cytoplasm of a model COS-1 cell line [28]. For NPs with $d > 16$ nm, cellular uptake is prohibited and NPs are found at the cellular periphery [28]. However, in other experiments, the PEGylated Au NPs with $d = 15 - 50$ nm were efficiently internalized by cancer cells [19,30,31]. Therefore, there exists a critical question: *What are the design criteria for PEGylated NPs to be quickly accepted by diseased cells?*

In the design of PEGylated NPs, there are two basic design parameters for grafted PEG polymers: one is the number of monomers per chain, N; the other is grafting density σ_p. These two parameters govern the surface morphology of PEGylated NPs as well their performance in the drug delivery process. However, experimental studies reported a varying range of these two parameters. For example, the typical molecular weight of grafted PEG polymer is about 550–5000 Da, corresponding to $N = 12$–112 [26–30,32,33]. The reported grafting densities of PEG polymers are within the range $\sigma_p = 0.2 - 2.0$ chains/nm^2 [26–30,32,33]. It is therefore not surprising that different experiments report seemingly contradictory findings for internalization behaviors of PEGylated NPs, as they use different combinations of N and σ_p.

Although the above-mentioned experiments have uncovered critical information about large scale interactions between PEGylated NPs and cells, many atomic-level questions remain to be answered, as they cannot be easily addressed by experiments. For instance, the conformational and structural properties of PEGylated NPs and their effects on drug delivery efficacy are difficult to be resolved by experiments. To understand the role of grafted PEG polymers during endocytosis, and in particular the effects of N and σ_p, we have performed large scale dissipative particle dynamics (DPD) simulations on internalization of PEGylated NPs. Existing studies primarily focused on first-generation NPs, eventually augmented with targeting moieties [8–10,13,15–17]. Our simulation results reveal that the endocytosis of PEGylated NPs heavily depends on both N and σ_p. Especially, the free energy change of grafted PEG polymer can play an important role during the endocytosis process, which apparently remained unnoticed in previous studies.

Section 2 describes the model and methods to simulate the endocytosis process of PEGylated NPs as well as the self-consistent field (SCF) theory to quantify the free energy change of PEG polymers. Section 3 contains the results from our DPD simulations and SCF analysis, and illustrates how the endocytosis process can be affected by the N and σ_p. Section 4 discusses the findings of the current work and compares them with experimental observations. Conclusions are drawn in Section 5.

2. Model and methodology

2.1. DPD simulation details

The coarse-grained molecular dynamics simulations adopted in this work are based on the DPD technique, a Lagrangian method developed for mesoscale simulations with hydrodynamic interactions. DPD has been successfully and widely used to study the behavior of biomembranes [20,22,34–36]. To model a large piece of lipid bilayer efficiently, we adopt the lipid model developed by Groot and Rabone [34]. In this model, the lipid molecule is represented by the $H_3(T_5)_2$ model (Supporting Information (SI) Sections 1.1, 1.2 and Fig. S1), where H and T denote the hydrophilic lipid heads and hydrophobic lipid tails, respectively. In the snapshots, the hydrophilic heads and hydrophobic tails are represented by the ice-blue beads and silver lines, respectively. The bending modulus and viscosity of the self-assembled lipid bilayer are found to agree reasonably well with experimental measurements [34]. Moreover, such a model has been successfully applied to study the translocation and endocytosis of different NPs [16,20–22,35,37]. In modeling the lipid bilayer, we assume that there are ~50% lipids coated with receptors to accelerate the DPD simulations, which has been proven to be a useful estimate in previous works [15,20,21]. The heads of these lipids attract the targeting moieties conjugated at the free ends of grafted chains, as described in SI Sections 1.3 and 1.4. These lipids are randomly distributed within the membrane. All the DPD simulations are performed in the NVT ensemble with time step $\Delta t = 0.01$ (dimensionless Lennard-Jones unit).

To maintain the zero lateral tension of the lipid bilayer during the DPD simulation, we adopted the N-varied DPD method to mimic a real cell membrane with large area-to-volume ratio [38]. In the N-varied DPD method, the lateral tension is maintained by monitoring the lipid number per area (LNPA) of the membrane, instead of the lateral force/pressure. The boundary region of the lipid membrane behaves like a reservoir of lipids in the DPD simulations. The LNPA of the boundary region is kept constant by adding/deleting lipid molecules. Simultaneously, the corresponding number of solvent beads is deleted/added to maintain the particle density of the whole system. Note that LNPA is directly related to the area per lipid. Thus, the N-varied DPD method offers an easy way to control lateral tension of membrane and supplies excess membrane area to release the tension induced by the internalization of PEGylated NPs. The N-varied DPD method has been successfully adopted to study the budding behaviors of multicomponent membranes [38], internalization of ligand-coated rigid NPs [39,40], as well dendrimer-like soft NPs [37]. More details are given in SI Section 1.5.

The core of our PEGylated NP is formed by 1566 close-packed 'beads' arranged on a FCC lattice circumscribed by a sphere of diameter $d = 8$ nm. The lattice constant is $\alpha \simeq 0.90$ nm. The close

packing prevents water and other beads to enter the interior of the core. During the DPD simulation, all the beads comprising the core move as a rigid body. PEG polymers are permanently grafted at randomly selected surface beads in accord with the given σ_p. For simplicity, a coarse-grained model established for PEG polymers [41] has been adopted in our DPD simulation. Within this model, each PEG monomer has been coarse-grained into a single bead. All these beads are consecutively connected by harmonic springs. The bending energy of a trimer, formed by three successive connected beads, is also considered in order to maintain the backbone stiffness of PEG [41]. Such a polymer model in our DPD simulations can correctly reproduce the radius of gyration and end-to-end distance of PEG polymers with different molecular weights obtained from all-atomistic and coarse-grained simulations, as reported by Lee et al. [41] (Fig. S2 in SI). The interaction parameters between PEG and lipid molecules are calibrated against experimental results (Table. S1 in SI), as discussed by Groot and Rabone [34]. Note that the PEG polymer is hydrophilic and its repulsive interaction with lipid tail (hydrophobic) is much larger than that with lipid head (hydrophilic).

We investigate a homologous series of grafting densities $\sigma_p \approx$ 0.2, 0.4, 0.6, 0.8, 1.0, 1.2, 1.4 and 1.6 chains/nm^2, corresponding to an integer-valued number $M = \pi d^2 \sigma_p = 40$, 80, 121, 161, 201, 241, 281 and 322 tethered chains, as shown in Fig. 1. Note that the different grafting densities σ_p considered in this work are within the range of experimentally studied grafting densities of PEG polymers, i.e. 0 (ungrafted) to 2.0 PEG/nm^2 [28,31,33]. It is known that PEGylation can reduce the interaction strength between NPs and the cell membrane due to a hydrophilic stealth shell formed around the NP surface. Thus, the cellular uptake of PEGylated NPs is prohibited because of the inability of the NP-membrane interaction to overcome the steric hindrance of PEG polymers. To include this mechanism, targeting moieties (ligands) are covalently bonded to the free ends of all grafted chains, allowing them to specifically recognize the expressed receptors over the cell membrane in the previous experiments [28–30,32]. The cellular uptake of PEGylated NPs is then greatly enhanced through specific ligand-receptor binding. To mimic this effect in our modeling, we consider that all free ends of grafted chains have attractive interactions with receptors coated on the heads of lipids (see Fig. 1 and SI Section 1.4). These attractive interactions have been well defined in the previous computational studies to mimic the specific ligand-receptor interactions [15,20,42,43].

2.2. Self-consistent field theory

We employ the SCF theoretical approach [44,45] to estimate the volume fraction profiles for each of the N monomers along a representative tethered chain separately. The SCF result allows us to calculate the radial volume fraction profile $\phi(r)$ of the spherical brush, the volume fraction profile of the terminal monomers, $\phi(r)$, and the corresponding free energy, F_p. We find that the measured PEG profiles are recovered using a simplest classical model of a polymer under good solvent conditions, that is characterized by a dimensionless mixing free energy density $\nu f_m(\phi) = \tau\phi^2 + w\phi^3$ with $\tau = w = 1$, where $\nu = 0.0633$ nm^3 denotes the excluded volume of a PEG monomer. Within the SCF we basically aim at minimizing a single chain free energy functional that is composed of an elastic and interaction part,

$$\frac{F_p}{k_B T} = \frac{3}{2}\frac{\langle r_{ee}^2\rangle}{R_0^2} + \int f_m(\phi) d^3 r \qquad [1]$$

where $\langle r_{ee}^2\rangle = V^{-1}\int (r - d/2)^2 \phi \mathrm{d}^3 r$ is the mean squared extension of a polymer that is tethered on a sphere of diameter d, properly normalized by the occupied chain volume $V = \int \phi \mathrm{d}^3 r = N\nu$, and $R_0 = R_0(N)$ stands for the equilibrium size of a PEG polymer, that is intermediate between its gyration radius and mean squared end-to-end distance. We employ $R_0^2 = \langle R_{ee}^2\rangle/e$ using the available $\langle R_{ee}^2\rangle(N)$ values for a single PEG chain in water (Fig. S2 in SI). The above free energy is minimized with respect to the volume fraction profile, subject to the constraints of conserved V and the tethering condition, $\phi(r < d/2) = 0$. A most common numerical implementation of the related optimization problem on a geometry-

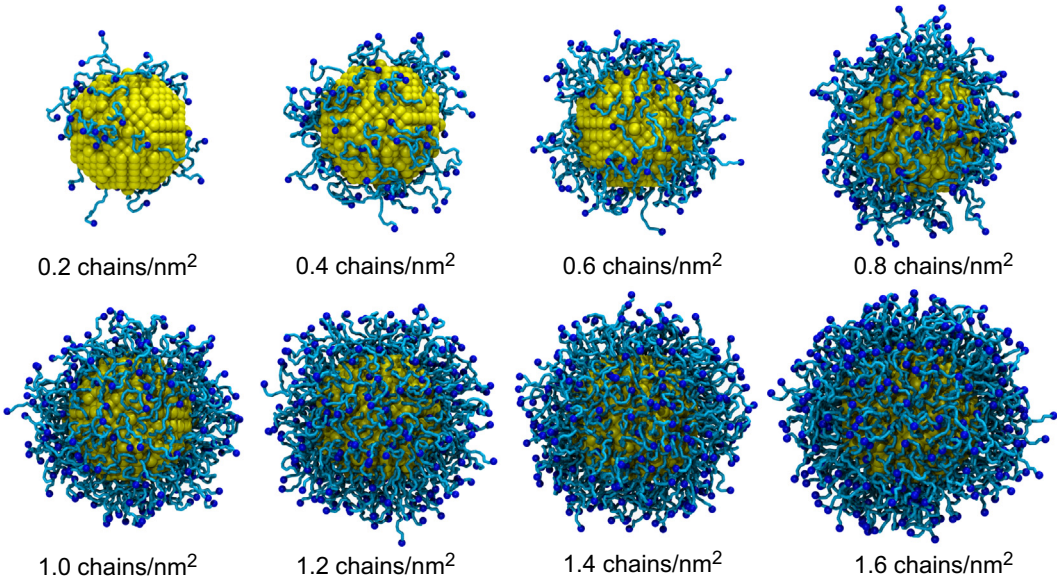

Fig. 1. Model setup for PEGylated NPs with different grafting densities σ_p. The diameter of the core is $d \approx 8$ nm and the PEG has $N = 18$ monomers, corresponding to a molecular weight of 838 Da. With σ_p increasing from 0.2 to 1.6 chains/nm^2, the conformation of grafted PEG polymers is transformed from the 'mushroom' to the 'brush' regime (see the detailed discussions in SI Section 2). The core of PEGylated NP is colored yellow. The PEG polymers and targeting moieties conjugated with free ends of the grafted chains are colored cyan and blue, respectively. These targeting moieties have attractive interactions with receptors attached to the heads of lipid molecules. For clarity, the solvent (water) molecules are not rendered here. (For interpretation of the references to colour in this figure legend, the reader is referred to the web version of this article.)

adapted grid had been introduced by Scheutjens and Fleer [46]. We follow the implementation described in detail by Wijmans and Zhulina [45]. To this end, a single flexible polymer is grown sequentially, using a constant bond length $a = 0.33$ nm (for PEG), starting from a spherical surface of diameter d. During (a priori) random growth within the space surrounding the nanoparticle, the representative chain creates its own radial volume fraction profile (with multiplicity of the number of tethered chains, recorded within spherical shells of thickness a) to which it reacts, as the volume fraction enters the probability to choose from all possible directions, at each step of the growth procedure. To be precise, it reacts by its current radial coordinate r to the dimensionless exchange chemical potential $U(\phi)/k_BT = vf'_m(\phi) = 2\phi + 3\phi^2$ contained in a segment weighting factor $G_1(r) = \exp(-U(r)/k_BT)$, where we recall that $\phi = \phi(r)$. The problem is thus closely related to a diffusion process in the presence of a potential and boundary, and can in principle also be formally treated using Green's functions. Accordingly, one introduces $G_n(r)$, the average statistical weight of an n-mer of which the last segment is located in layer r: $G_n(r) = G_{n-1}(r)G_1(r)$ for $n = 2, \ldots, N$, where the spatial average is taken over a sphere of radius a, centered at r. We are left with a closed set of coupled equations, where the averages play the role of the coefficients of a linear system of equations that can be solved in an iterative fashion using simple matrix inversions. Due to head-tail symmetry of the polymer chains, the volume fraction profile of an n-mer is subsequently obtained from the solution $G_n(r)$ via $\phi_n(r) = C_nG_n(r)G_{N-n+1}(r)/G_1(r)$, where the C_n's are normalization factors that follow from $v = \int \phi_n(r)\mathrm{d}^3r$ and finally $\phi(r) = \sum_{n=1}^{N}\phi_n(r)$ as well as $\phi_N(r)$ are obtained. Because the volume fraction profiles $\phi_n(r)$ of the unwrapped PEGylated NP are all well recovered (as given in the following section), we can estimate the free energy difference $F_{\mathrm{polymer}} = \Delta F_p$ between wrapped and unwrapped PEGylated NP upon inserting the two measured $\phi(r)$'s separately into Eq. (1).

3. Results

3.1. Morphology of PEGylated NPs

Before simulating the internalization pathway of PEGylated NPs, our NPs have been fully equilibrated in the water environment (configurations shown in Fig. 1). When σ_p is very small, the conformation of chains is in 'the mushroom' regime. However, when σ_p is high, their conformation is in the 'brush' regime (see SI Section 2 for a detailed discussion, and Eq. (2)). These observations are consistent with the theoretical results presented by Szleifer and Carignano [47]. These different conformations are directly related to the protein absorption capabilities of PEGylated NPs, which have been studied both theoretically and experimentally [33,48]. The endocytosis of PEGylated NPs can be greatly influenced by these different conformations as well. The particle density distribution functions of targeting moieties to the center of PEGylated NP are given in Fig. S5 of SI. When σ_p is very small, the targeting moieties are mostly distributed within the hydrophilic stealth shell and cannot effectively interact with the receptors. With increasing σ_p, more targeting moieties can be found outside of the stealth shell. Therefore, the PEGylated NPs with high grafting (ligand) densities can be more easily taken up by the cell due to strong ligand-receptor interactions.

The radius R of PEGylated NPs linearly increases with increasing σ_p, as can be seen in Table 1 and Fig. S6 of SI. The average volume occupied by a single grafted chain V_{polymer} is obtained by dividing the volume difference of the NP before and after PEGylation by the number of PEG chains per NP, $V_{\mathrm{polymer}} = (\pi/6)(8R^3 - d^3)/M$. As shown in Table 1, V_{polymer} decreases nonlinearly with the increment of σ_p, in contrast with the size of PEGylated NPs. The experimentally observed size of PEGylated Au NPs and V_{polymer} of grafted PEG chains [33] are found to be in good agreement with our DPD simulations (SI Section 2). These agreements further verify and validate our model for PEGylated NPs. Moreover, smaller values of V_{polymer} indicate a larger loss in conformational degrees of freedom by grafted PEG chains, which has also been observed in experiments [33]. This loss in conformational degrees of freedom can prevent water molecules from being absorbed by the grafted chain and can increase the thermodynamic barrier to serum protein adsorption [33,49], consistent with our observations of the conformational changes of grafted PEG polymers (Fig. 1).

Table 1
Effect of grafting density σ_p (or number of tethered chains, M) on the radius R of PEGylated NPs, the average volume V_{polymer} occupied by a single grafted chain, radius of gyration R_g, and end-to-end distance R_{ee} of grafted chains. The core diameter is 8 nm and the grafted PEG length is $N = 18$ (corresponding to molecular weight 838 Da). 'Before' and 'After' indicate the values for R_{ee} of grafted chains before and after endocytosis, which are calculated at ligand-receptor binding strength $\varepsilon_b = 6.2k_BT$. F_{polymer} represents the free energy change of grafted chains before and after endocytosis. The radius R is defined as the mean distance between targeting moieties and center of the PEGylated NP. V_{polymer} is obtained by dividing the volume difference of NPs before and after PEGylation by the number of grafted chains M.

Before endocytosis						After endocytosis	
σ_p Chains/nm^2	M	R[a] nm	V_{polymer}[a] nm^3	R_g nm	R_{ee} (before) nm	R_{ee} (after) nm	F_{polymer}[b] k_BT
0.2	40	5.69	12.56	0.99	2.66	N/A	N/A
0.4	80	5.82	6.96	0.99	2.67	2.93	10.00
0.6	121	5.98	5.20	1.01	2.74	2.77	41.86
0.8	161	6.16	4.41	1.02	2.82	2.89	78.07
1.0	201	6.31	3.90	1.04	2.89	2.96	83.29
1.2	241	6.46	3.57	1.05	2.96	2.90	156.18
1.4	281	6.60	3.34	1.07	3.04	2.90	120.47
1.6	322	6.76	3.19	1.08	3.13	3.04	120.83

[a] The R and V_{polymer} of these NPs are found to be in good agreement with experimental results [46], as discussed in SI Section 2.
[b] F_{polymer} is calculated based on the self-consistent field theory, according to Eq. (1).

The results on grafted chains' radii of gyration R_g and end-to-end distances R_{ee} further confirm our above observations (Table 1). At high grafting densities, the PEG chains are more stretched and flattened for larger R_g and R_{ee} values due to their steric (repulsive) interactions. Note that $R_{ee}^2 = 6R_g^2$ for equilibrium chains with random coil conformations. However, $R_{ee}^2 > 6R_g^2$ in the grafted state, as shown in Table 1, which also indicates that the conformation of chains has been dramatically changed. Changes in the conformational degrees of freedom of grafted PEG polymers are directly related to their free energies.

Within the SCF theory that we use to calculate detailed information about the underlying volume fraction $\phi(r)$ of PEG chains within the corona of the NPs, the free energy of a single chain consists of an elastic and interaction part, cf. Eq (1), that can be rewritten as,

$$\frac{F_p}{k_BT} = \frac{3}{2}\frac{\langle r_{ee}^2\rangle}{R_0^2} + N\langle\frac{vf_m(\phi)}{\phi}\rangle = \frac{3}{2}\frac{\langle r_{ee}^2\rangle}{R_0^2} + \tau N\langle\phi\rangle + \ldots \qquad [2]$$

since averages are calculated with the yet unknown volume fraction profile $\phi(r)$ via $\langle A\rangle = \int A\phi\mathrm{d}^3r/\int\phi\mathrm{d}^3r$. The free energy expression Eq. (2) reduces to the more familiar Flory free energy within the strong stretching assumption, where $\langle r_{ee}\rangle = R_{ee}^2$, and where $\phi = \phi(r)$ is considered to be the spatially homogeneous ratio between occupied, Nv, and accessible volume per single chain. The accessible volume $V_d(R_{ee})$ of a PEG chain tethered to a spherical NP of diameter d is the Mth fraction of the corona volume,

$V_d(R_{ee})\sim[8(R_{ee}+d/2)^3-d^3]/M$. Inserting these particular $\langle r_{ee}^2\rangle$ and $\phi = Nv/V_d(R_{ee})$ into Eq. (2) yields

$$\frac{F_p}{k_BT}=\frac{3}{2}\frac{R_{ee}^2}{R_0^2}+\tau N\frac{Nv}{V_d(R_{ee})} \simeq \frac{3}{2}\frac{R_{ee}^2}{R_0^2}+\begin{cases}\tau N\dfrac{Nv}{R_{ee}^3}+\ldots & \left(R_{ee}^2<1\Big/\sigma_p:\text{mushroom}\right)\\ \tau N\dfrac{Nv}{R_{ee}/\sigma_p}+\ldots & \left(R_{ee}^2>1\Big/\sigma_p:\text{planar brush}\right)\end{cases} \quad [3]$$

where we explicitly mentioned in Eq. (2) the limiting mushroom (single free chain, $M=1$, $R_{ee}^2<1/\sigma_p$) and planar brush ($R_{ee}^2>1/\sigma_p$) special cases of the more general Flory-type expression. Under ideal good solvent conditions, $\tau>0$ and higher order virial coefficients are of minor relevance. In that extremal case F_p is readily minimized with respect to R_{ee} to obtain the equilibrium R_{ee} for the unconfined, unwrapped PEGylated NP as function of N and σ_p [50]. While the Flory approach yields an analytic result that can be used as a first approximation for a hydrophilic polymer like PEG in water, its assumptions are not met for the realistic scenario under study; in particular the chains are not fully stretched, $\phi(r)$ is not a constant, and the third virial coefficient w cannot be neglected. Moreover the situation is more complex as we are faced with a curved tethering surface. These aspects are fully taken into account within the unapproximated SCF that we apply to a PEGylated NP (Section 2.2). The simple Eq. (2) serves to highlight that the free energy of grafted PEG chains is highly dependent on the end-to-end distance R_{ee}. This aspect will be further discussed in the following part.

3.2. Internalization pathway of PEGylated NPs

Fig. 2 shows the representative receptor-mediated endocytosis pathway of PEGylated NPs. Depending on the position of the PEGylated NP, the wrapping process can be divided into three stages: membrane bending stage ($0<t<122$ ns), membrane monolayer protruding stage ($122\text{ ns}<t<750$ ns) and equilibrium stage ($t>750$ ns). During the membrane bending stage, the targeting moieties conjugated at free ends of the grafted PEG chains recognize and bind to the receptors (lipid heads) sitting in the membrane. Simultaneously, the membrane starts to bend and to wrap around the PEGylated NP. With time increasing, more and more receptor molecules diffuse into the membrane bending region and form bindings with targeting moieties on PEGylated NP. In this stage, the energy released by the ligand-receptor binding provides the major driving force for the membrane to bend and wrap around the PEGylated NP, until the wrapping process enters the second stage. At the time $t\approx 122$ ns, the majority of the PEGylated NP is wrapped by the membrane and the upper leaflet of the membrane starts to protrude and wrap the PEGylated NP from the top. The lower leaflet of the membrane, however, bends slowly and weakly, compared with its performance during the first stage

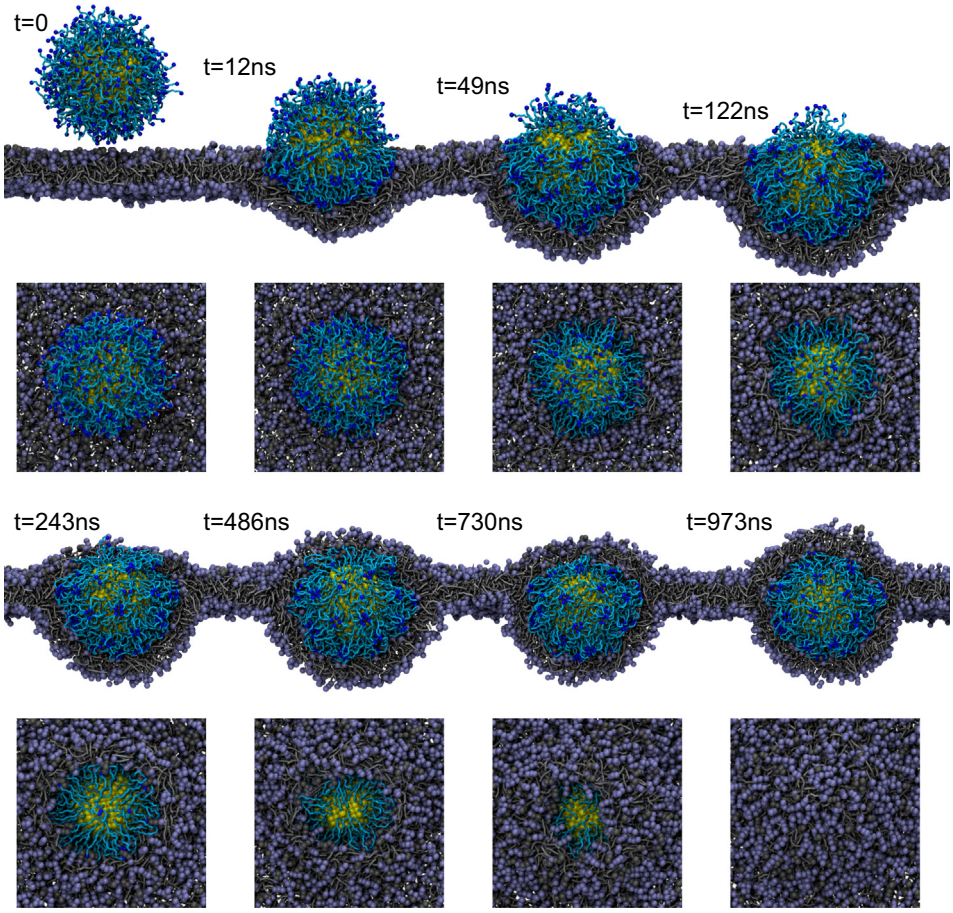

Fig. 2. Representative DPD simulation snapshots for endocytosis of PEGylated NP with core diameter $d\approx 8$ nm. The whole process can be classified into three stages: membrane bending stage ($0<t<122$ ns), membrane monolayer protruding stage ($122<t<750$ ns) and equilibrium stage ($t>750$ ns). The grafting density of PEG with $N=18$ is $\sigma_p=1.6$ chains/nm^2. The ligand-receptor binding strength is $\varepsilon_b=6.2k_BT$. The color scheme is the same as Fig. 1. The hydrophilic heads and hydrophobic tails of lipids are represented by ice-blue beads and silver lines, respectively. The lipid heads coated with receptors are represented by gray beads. For clarity, the solvent (water) molecules are not rendered.

(membrane bending stage). Later on, the PEGylated NP is slightly pulled upwards and located around the center of membrane to reduce the bending energy penalty of the lower membrane monolayer. At $t \approx$ 750 ns, the PEGylated NP is fully and symmetrically wrapped between the upper and lower leaflets of the membrane. A similar wrapping pathway has been found for hydrophilic NPs decorated by ligands only (without PEGylation) [21,40,51].

Here we should emphasize that the protrusion of the upper leaflet of the membrane is induced by the strong ligand-receptor binding and the high fluidity of the lipid bilayer, as discussed by Yue et al. [40]. The monolayer protrusion regulated wrapping can be further transformed to the complete internalization, through a small amount of external force (e.g 6.4 pN) [40], induced by actin filaments in the cell [52] or actin polymerization [3,53].

The internalization rate is strongly dependent on the grafting (ligand) density σ_p of PEG polymers. The wrapping ratio, defined as the wrapped area fraction of the PEGylated NP, is plotted versus endocytic time in Fig. 3. At ligand-receptor binding strength $\varepsilon = 6.2k_BT$, most of the PEGylated NPs can be internalized within 4000 ns, except the PEGylated NP with low $\sigma_p = 0.2$ chains/nm^2. Similar to the internalization pathway shown in Fig. 2, these PEGylated NPs are symmetrically enveloped by the membrane at the last stage of the process. Moreover, the wrapping speed slows significantly with decreasing σ_p. When $\sigma_p \leq 0.2$ chains/nm^2, the PEGylated NP can only be partially wrapped by the membrane, even after 5000 ns, as given in the snapshots of Fig. 3 and Fig. S7 in SI.

3.3. Free energy change during endocytosis

When the PEGylated NP interacts with the cell membrane, there are three major contributions to the free energy of the system, F. The first is the bending energy F_{memb} of the membrane, which is related to the curvature change of the membrane during endocytosis. The second is the specific ligand-receptor interaction F_{ligand}. The third is the non-specific free energy $F_{polymer}$ of the grafted PEG chains due to the steric (repulsive) interactions between grafted chains and the membrane. Thus, $F = F_{memb} + F_{ligand} + F_{polymer}$. Note that the free energy changes induced by the thermal fluctuations of the membrane and entropy loss of translation associated with receptors are much smaller than these three major contributions [54,55]. Therefore, these terms are ignored in calculating the free energy change of the whole system F. During endocytosis, as shown in Fig. 2, the membrane curvature change will enlarge F_{memb}. At the same time F_{ligand} will be reduced due to the ligand-receptor binding. However, a more subtle question is *To what extent does the free energy $F_{polymer}$ of the grafted PEG polymers change?* As we learned from $V_{polymer}$ in Table 1, when the PEG chains are grafted to the core of a NP, they lose conformational degrees of freedom. Their corresponding entropy ΔS reduces, while increasing the free energy of PEG chains as $F_{polymer} = -T\Delta S$ (T is the temperature). Similarly, when the PEGylated NP is wrapped by the membrane, the conformational degrees of freedom of the PEG chains are further reduced as they are now confined between the core of the NP and the membrane. Hence $F_{polymer}$ can be greatly enlarged, when the PEGylated NP is enclosed within the membrane. Therefore, during endocytosis of the PEGylated NPs, both F_{memb} and $F_{polymer}$ are increased, while F_{ligand} is decreased, providing the driving force for PEGylated NP to be internalized. The reduction of F_{ligand} should be larger than the increment of F_{memb} and $F_{polymer}$. Otherwise, the endocytosis cannot occur spontaneously. Note that here we study the ligand-receptor mediated endocytosis of NPs. The thermodynamic driving force is the ligand-receptor binding, which does not necessarily require either the expenditure of ATP or the presence of lipid rafts [8,9,15]. Since the free energy changes of membrane bending F_{memb} and ligand-receptor binding F_{ligand} during endocytosis have been extensively studied in the previous works [8–10,18,56,57], we will briefly discuss them in the following part, and mainly focus on the free energy change of grafted PEG polymer $F_{polymer}$.

The free energy change F_{memb} induced by the curvature change of the membrane can be analytically quantified, which has been discussed in the previous works [8–10,18,37,56–58]. Compared with its flat counterpart, the free energy of the membrane wrapped around a NP surface is $F_{memb} = 8\pi\kappa$ [56,57], obtained by integrating the curvature over the spherical NP and ignoring the contributions from surface roughness of the monolayer. Here $\kappa \approx 10k_BT$ is the bending rigidity of the model membrane [36,37]. Therefore, $F_{memb} \approx 251k_BT$, regardless of the size of wrapped PEGylated NP. Here we should emphasize that the model membrane is only formed by phospholipids, which mimics the behavior

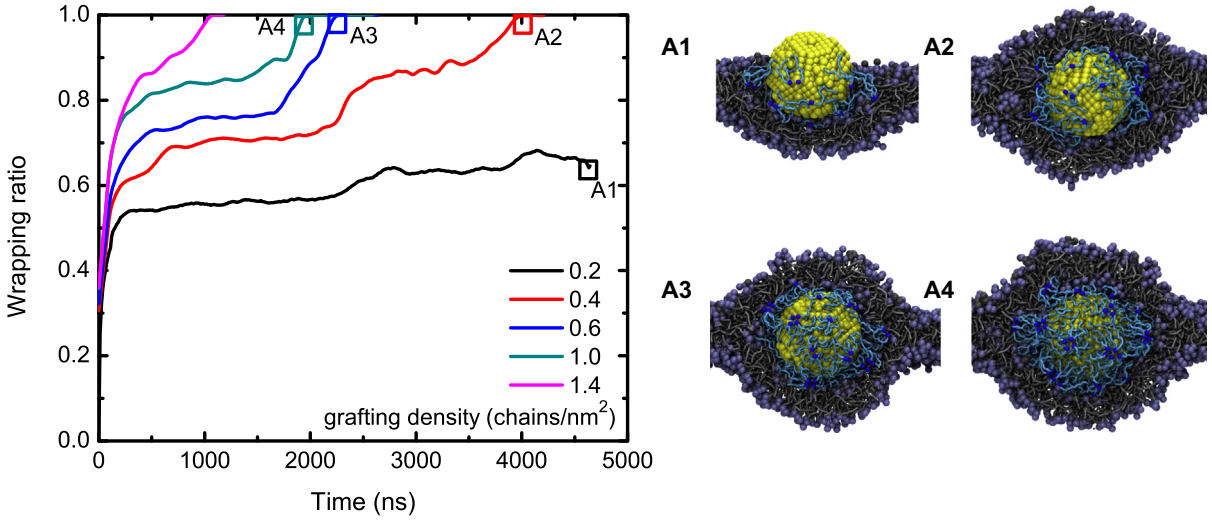

Fig. 3. Effect of grafting density on the wrapping ratio of PEGylated NPs. The core diameter of PEGylated NPs is 8 nm with grafted PEG of $N = 18$. The ligand-receptor binding strength is $\varepsilon_b = 6.2k_BT$. Wrapping ratios 0 and 1 denote the unwrapped and completely wrapped state, respectively. Snapshots for endocytosis of PEGylated NPs with different grafting densities, marked by A1-A4, are given on the right. The color scheme is the same as Fig. 2.

of pure 1-palmitoyl-2-oleoyl-sn-glycero- 3-phosphocholine (POPC) bilayer [22,35]. However, in the experiments, the cell membranes are more complicated, as they contain cholesterol and possibly skeletal proteins, and would be expected to be more rigid (larger value of κ) [59].

The free energy change F_{ligand} induced by ligand-receptor binding can also be analytically calculated. The binding strength ε_b is related to the ligand-receptor interaction potential $U_{ij}^{\text{ligand-receptor}}$ defined in our DPD simulations. The relationship between binding strength ε_b and energy well depth $\varepsilon_{\text{ligand-receptor}}$ in $U_{ij}^{\text{ligand-receptor}}$ is given in SI Section 1.4 and Fig. S3. Accordingly, $F_{\text{ligand}} = M\varepsilon_b$ when the PEGylated NP is internalized by the cell, where M denotes the number of targeting moieties per NP, as we consider that all the free ends of grafted PEG chains are conjugated with targeting moieties, which mimics the experimental condition [29,30,32,33].

As is evident from Eq. (2), the free energy change F_{polymer} of grafted chains is captured by their end-to-end distance R_{ee} during the endocytosis. To understand this effect, we monitor the change of chain's end-to-end distance R_{ee} during endocytosis process (SI Section 3 and Fig. S8). For different grafting densities, we find that the R_{ee} can be slightly enlarged during the initial stage, as the free ends of grafted PEG chains are stretched out to bind with the receptors on the cell membrane. However, after the PEGylated NPs have been fully wrapped by the membrane, the R_{ee} suddenly drops to a smaller value, due to the confinement induced by the cell membrane. All these changes of R_{ee} indicate a free energy change F_{polymer} of grafted PEG polymers, before and after endocytosis, which needs to be understood in detail.

To quantify the free energy change of grafted PEG polymers, we adopt the SCF theory developed for polymer brushes (Eq. (1)). From the SCF calculation, the volume fraction profiles of both grafted PEG polymers and their free ends can be directly predicted before the PEGylated NP is wrapped by the membrane. As shown in Fig. 4, the volume fraction profiles $\phi(r)$ of grafted PEG polymers and their free ends can also be directly calculated from our DPD simulations. In Fig. 4a, the $\phi(r)$ profiles predicted by the SCF calculations are given as solid lines. Interestingly, the volume fractions given by our DPD simulations are in good agreement with the SCF calculation results, except for $\phi(r)$ close to the surface of the core ($r \simeq 4$ nm). As we learn from the snapshots of PEGylated NPs (Fig. 1), the core of the PEGylated NP is not a perfect sphere, as it was formed by beads arranged on a FCC lattice. However, in our SCF calculations, we assume that the core of the NP is a perfect sphere. Due to this tiny difference, the $\phi(r)$ profiles given by DPD simulations slightly deviate from the SCF predictions, when $r \simeq 4$ nm (around the surface of the core). We should emphasize that the $\phi(r)$ profiles for the unwrapped PEGylated NPs with grafting densities $\sigma_p = 0.4 - 1.6$ chains/nm^2 are all well recovered by the SCF calculations (SI Fig. S9) without changing any parameter except for σ_p. In light of these agreements, the free energy difference F_{polymer} of grafted PEG polymers, before and after endocytosis, can now be directly estimated upon inserting the two measured $\phi(r)$ profiles, from wrapped and unwrapped PEGylated NP, into Eq. (1).

According to the SCF calculation (Eq. (1)) and the volume fraction profiles $\phi(r)$ given by the DPD simulations, the free energy per monomer of grafted chains F_p/Nk_BT is plotted in Fig. 5a. F_p/Nk_BT is monotonically increasing with the number of grafted chains (grafting density) increasing, not matter before or after endocytosis, in agreement with the changes of V_{polymer} (Table 1). Moreover, the value of F_p/Nk_BT has been enlarged, when the PEGylated NP has been taken up the cell, as we expected from above discussions. Taking the free energy difference of F_p/Nk_BT shown in Fig. 5a, the free energy change F_{polymer} of PEG polymers during endocytosis is immediately available and shown in Fig. 5b (also listed in Table 1). Due to the different numbers of grafted PEG chains, F_{polymer} varies from 10 to 156 k_BT for $N = 18$. As we mentioned in the above discussion, the free energy change induced by membrane bending is about $F_{\text{memb}} \simeq 251k_BT$ (dashed line in Fig. 5b). Thus, the free energy change F_{polymer} of grafted PEG polymer during the internalization process is found to be comparable with F_{memb} when the grafting density is large. We should emphasize that in the previous studies, the primary focus in the study of the endocytosis process was placed on the free energy change of the membrane F_{memb} and ligand-receptor interaction F_{ligand} only [8,9,18,37]. With the current study we provide evidence that F_{polymer} is important as well, and eventually comparable in magnitude with F_{memb}. Therefore, in the design of PEGylated NPs, the contribution of F_{polymer} should be taken into account. A similar conclusion about the relevance of the polymer contribution was recently put forward in the study of mechanisms of harvesting cells cultured on thermoresponsive polymer brushes [60,61].

From the above analysis, the free energy change of the whole system F is obtained. For a given σ_p , there exists a critical binding strength ε_b for which $F = 0$. Beyond this critical value, complete wrapping of the PEGylated NP is energetically favorable. The

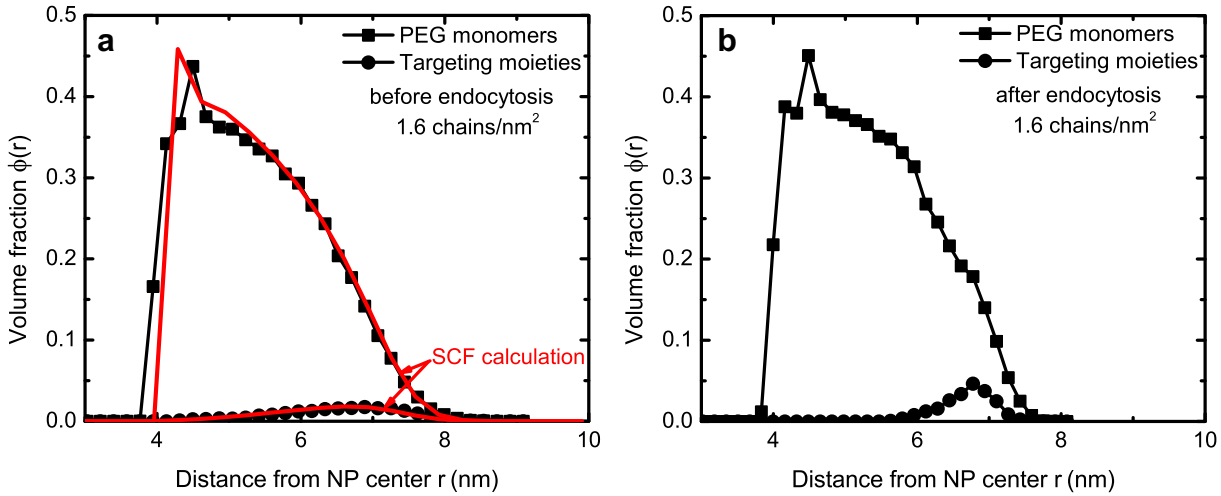

Fig. 4. Volume fraction profiles $\phi(r)$ of grafted PEG polymers and their free ends (conjugated with targeting moieties) for a PEGylated NP: (a) before endocytosis and (b) after endocytosis. The core diameter of PEGylated NP is about 8 nm, grafted with $N = 18$ at $\sigma_p = 1.6$ chains/nm^2. In (a), the solid lines are given by the SCF calculations.

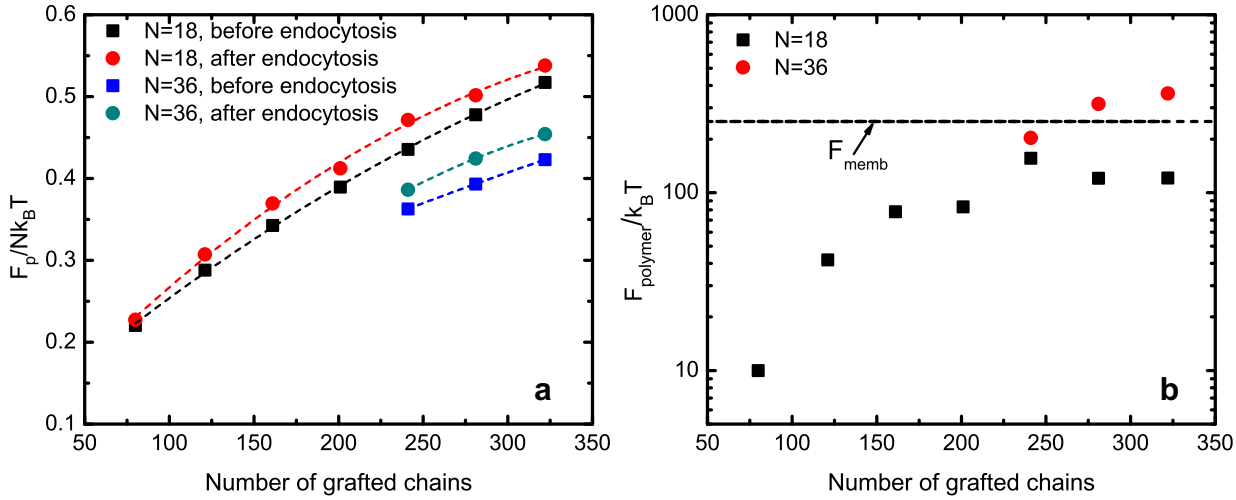

Fig. 5. Free energy change of grafted PEG polymers during endocytosis: (a) free energy per monomer F_p/Nk_BT and (b) free energy change of all grafted chains $F_{polymer}$. In (a), the dashed lines guide eyes. In (b), the bending energy change of membrane is $F_{memb} \simeq 251k_BT$.

predicted critical values of ε_b are given as the dashed line in Fig. 6. To further confirm our analytical predictions, we ran simulations with different ligand-receptor binding strengths ε_b. According to the different values of ε_b, the final trajectories of DPD simulations can be grouped into two classes: fully wrapped and partially wrapped regimes. The simulation results agree well with our theoretical predictions only if $F_{polymer}$ is taken into account, as demonstrated in Fig. 6.

3.4. Effect of grafted PEG molecular weight

As previously mentioned, the molecular weight of grafted PEG polymers typically varies between 550 and 5000 Da [26–30,32,33]. To understand the effect of N, we study another set of PEGylated NPs with larger N. The core of the NP is still about 8 nm, while the grafted PEG has $N = 36$ monomers (corresponding to molecular weight 1630 Da), twice its value of the previous case (their conformations are given in Fig. S10 of SI). Due to the limit of computation, the larger values of N are not considered in current work. The radius R of PEGylated NPs and average volume $V_{polymer}$ per chain are given in Table 2. Again, we find that R increases linearly with σ_p, while $V_{polymer}$ decreases nonlinearly with σ_p (SI Fig. S11). All these observations are in good agreement with the PEGylated NPs with lower degree of polymerization, $N = 18$ (Table 1), and experimental observations on PEGylated Au NPs [33]. Comparing with the previous PEGylated NPs ($N = 18$), the radius R for PEGylated NPs with $N = 36$ has been increased by about 2 nm for a given σ_p. Such an increment may have an impact on the internalization rate of PEGylated NPs (to be discussed below).

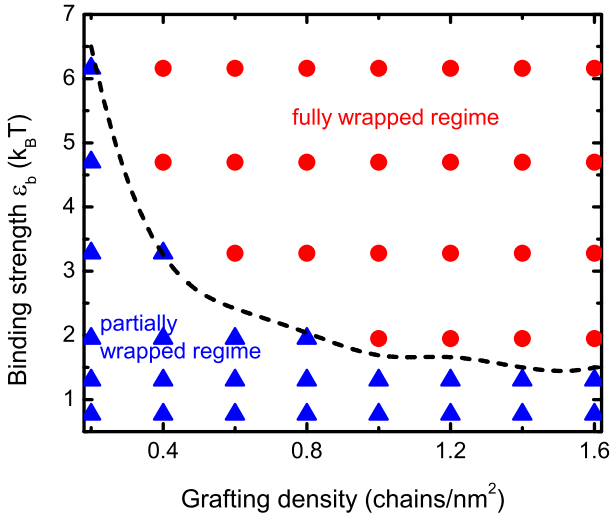

Fig. 6. Phase diagram of receptor-mediated endocytosis of PEGylated NPs, obtained from DPD simulations and theoretical predictions. The phase diagram is given as a function of the ligand-receptor binding strength ε_b and σ_p. The results are classified into partially wrapped (▲ symbols) and fully wrapped regimes (● symbols). The core diameter of PEGylated NPs is 8 nm and $N = 18$. The dashed line is predicted by considering the balance between F_{memb}, $F_{polymer}$ and F_{ligand}.

Fig. 7 shows the internalization pathway for a PEGylated NP with $\sigma_p = 1.6$ chains/nm^2 and $N = 36$. Similar to the PEGylated NPs with shorter grafted chains (see Fig. 2), the endocytosis process can be classified into three stages: membrane bending stage ($0 < t < 1946$ ns), membrane monolayer protruding stage ($1946 < t < 5000$ ns) and equilibrium stage ($t > 5000$ ns). In the course of this process, the R_{ee} of grafted PEG polymers initially increases monotonically with time (Fig. S12 of SI), as the targeting moieties conjugated with free ends of tethered chains bind with receptors on the membrane. Before the PEGylated NP is wrapped by the membrane, the targeting moieties are hidden inside of the tethered layer of PEG polymer to minimize the free energy $F_{polymer}$. When the PEGylated NP is wrapped by the membrane, the grafted PEG polymers are stretched out to bind with the receptors in the membrane, significantly reducing F_{ligand}. The energy released by the ligand-receptor binding provides the driving force for the bending of the membrane and the stretching of grafted PEG polymers. Until the PEGylated NP is fully wrapped by the membrane, R_{ee} drops to a smaller value to reduce the free energy $F_{polymer}$. Comparing the R_{ee} values before and after endocytosis, the grafted chains are more stretched for $N = 36$ than that of $N = 18$. Such a difference indicates a dramatic change of free energy of grafted PEG polymers with $N = 36$ (cf. Eq. (2)). Besides, in contrast to $N = 18$, there are other distinct features for PEGylated NPs with $N = 36$.

First, the internalization rate of PEGylated NPs is greatly affected by N. The wrapping ratio of PEGylated NPs with $N = 36$ is shown in Fig. 8. Comparing with the shorter $N = 18$ chains (Fig. 3), the internalization rate of PEGylated NPs is significantly slowed down due to the increase of N. For example, when $\sigma_p = 1.4$ chains/nm^2 it

Table 2
Effect of grafting density σ_p (number of grafted chains M) on the radius R of PEGylated NPs, average volume $V_{polymer}$ occupied by a single grafted chain, radius of gyration R_g, and end-to-end distance R_{ee} of grafted chains. The core diameter is 8 nm and the grafted PEG length is $N = 36$ (corresponding to molecular weight 1630 Da). $F_{polymer}$ represents the free energy change of grafted chains before and after internalization.

Before endocytosis						After endocytosis	
σ_p Chains/nm^2	M	R nm	$V_{polymer}$ nm^3	R_g nm	R_{ee} (before) nm	R_{ee} (after) nm	$F_{polymer}$ k_BT
0.2	40	6.66	24.28	1.52	4.02	N/A	N/A
0.4	80	7.03	14.81	1.55	4.20	N/A	N/A
0.6	121	7.36	11.60	1.59	4.38	N/A	N/A
0.8	161	7.62	9.83	1.62	4.51	N/A	N/A
1.0	201	7.91	8.97	1.66	4.70	N/A	N/A
1.2	241	8.13	8.22	1.69	4.82	5.37	203.21
1.4	281	8.39	7.86	1.74	5.01	5.31	315.47
1.6	322	8.60	7.44	1.77	5.15	5.31	361.05

takes about 1000 ns for PEGylated NPs with $N = 18$ to be fully wrapped. However, the wrapping time is increased to 6000 ns for $N = 36$. Thus, the wrapping time is increased by a factor 6, while N is doubled. As we have noticed, the radius R of PEGylated NP is enlarged from 6.60 to 8.39 nm, as N is enlarged from 18 to 36. Therefore, the internalization rate of the PEGylated NP can be reduced by increasing its size [8,10,18]. In addition to this size effect, the free energy change of the grafted PEG polymers also plays an important role. Using our SCF calculations (SI Section 4), the free energy changes $F_{polymer}$ of longer grafted chains can be quantified as well (Table 2 and Fig. 5). For $\sigma_p = 1.4$ chains/nm^2, $F_{polymer} = 120.47k_BT$ and $315.47k_BT$ for $N = 18$ and 36, respectively. Upon doubling N, $F_{polymer}$ for $N = 36$ is about 2.6 times $F_{polymer}$ for $N = 18$. This previously ignored free energy penalty induced by longer grafted PEG polymers can further delay the internalization process of PEGylated NPs.

Second, the free energy change $F_{polymer}$ of grafted PEG polymers can be larger than the bending energy F_{memb} of the membrane and plays an important role during endocytosis. When $N = 18$, $F_{polymer}$ varies between 10 and $156k_BT$ depending on σ_p. However, for $N = 36$, $F_{polymer}$ varies between 200 and $360k_BT$, for $\sigma_p = 1.2$ to 1.6 chains/nm^2, and can thus exceed the bending energy of the membrane $F_{memb} = 251k_BT$ (see Fig. 5b). As previously mentioned, the grafted PEG chains can be as large as $N = 112$ with $\sigma_p = 1.2 - 1.6$ chains/nm^2 [33] for PEGylated Au NPs. Thus, we expect the free energy change $F_{polymer}$ to be further enlarged. In this

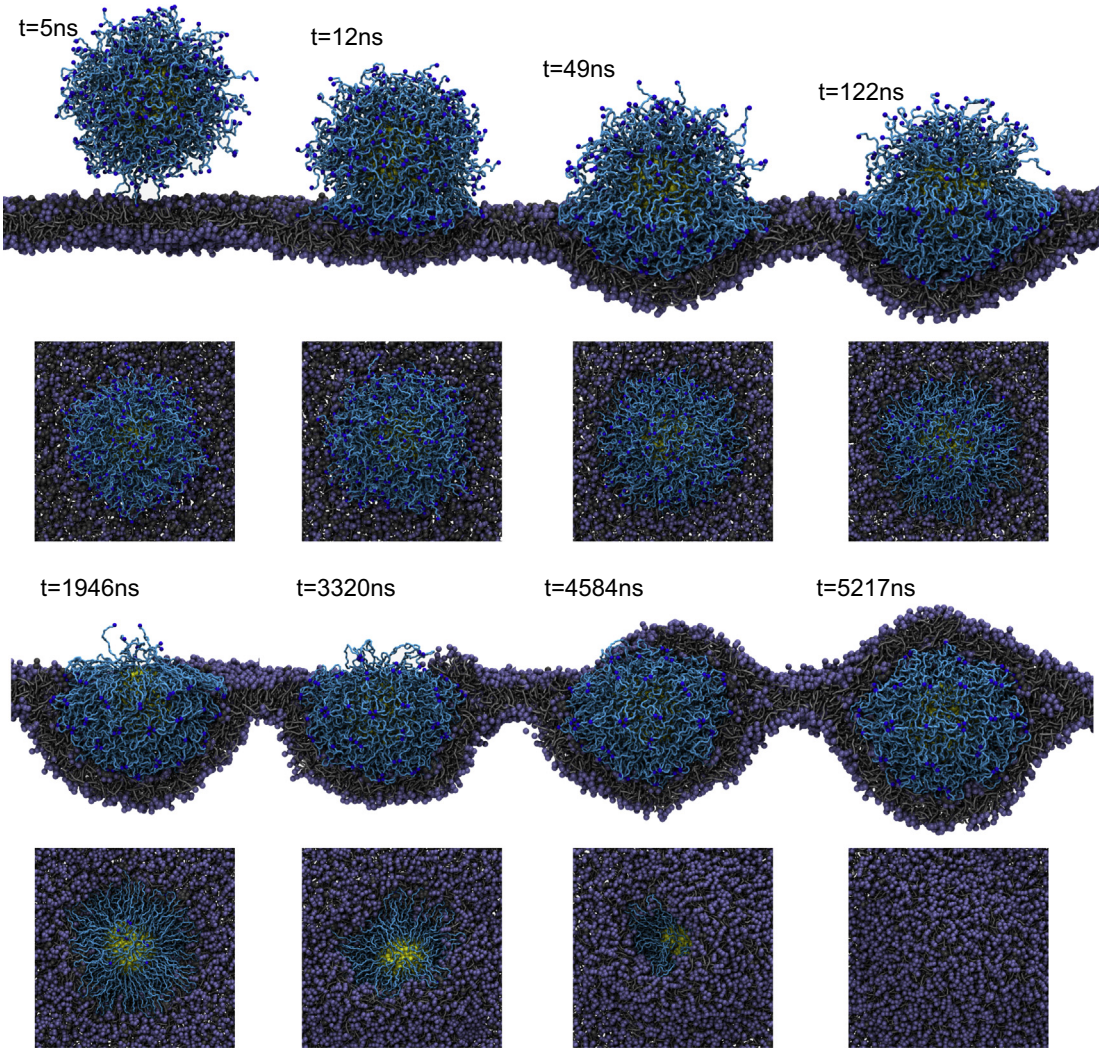

Fig. 7. Representative DPD simulation snapshots for endocytosis of PEGylated NP. The whole process can be classified into three stages: membrane bending stage ($0 < t < 1946$ ns), membrane monolayer protruding stage ($1946 < t < 5000$ ns) and equilibrium stage ($t > 5000$ ns). The core diameter of the NP is 8 nm, $\sigma_p = 1.6$ chains/nm^2 with $N = 36$ PEG. The ligand-receptor binding strength is $\varepsilon_b = 6.2k_BT$. For clarity, the solvent (water) molecules are not rendered. The color scheme is identical with the one chosen for Fig. 2.

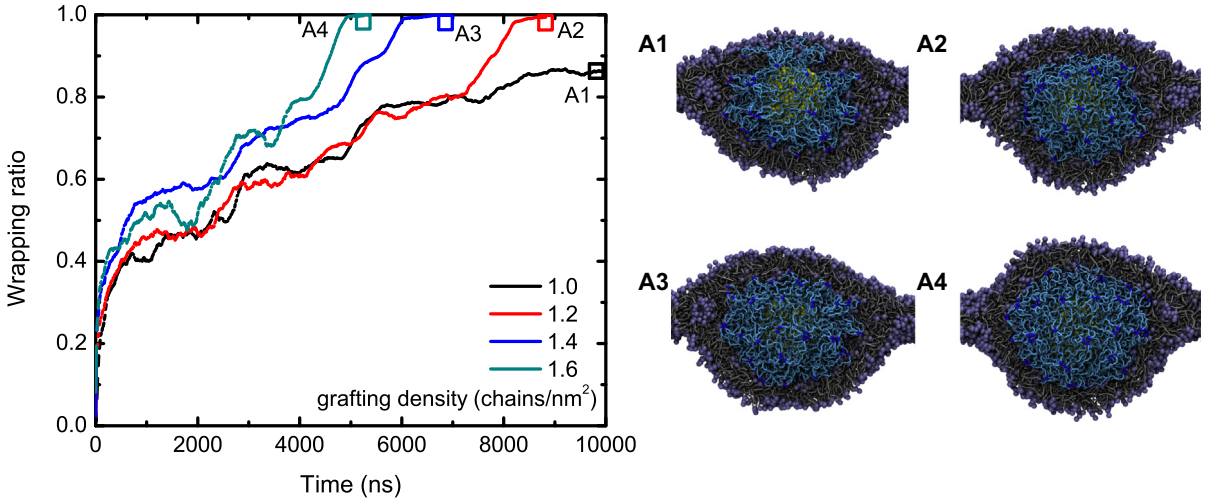

Fig. 8. Effect of grafting density on the wrapping ratio of PEGylated NPs. The core diameter of PEGylated NPs is 8 nm, grafted with $N = 36$ PEG. The ligand-receptor binding strength is $\varepsilon_b = 6.2k_BT$. Wrapping ratios 0 and 1 denote the unwrapped and completely wrapped states, respectively. The snapshots A1-A4 for endocytosis of PEGylated NPs with different grafting densities are given on right. The color scheme is as the same as that given in Fig. 2.

case, $F_{polymer}$ will be much larger than F_{memb} and will play the dominant role during the endocytosis. Ignoring the contribution of $F_{polymer}$ for designing PEGylated NPs may prohibit successful drug delivery as the PEGylated NPs cannot be fully wrapped by the membrane (cf. Fig. 6).

4. Discussion

The above simulation results and theoretical analysis may shed light on understanding and explaining the experimental observations on endocytosis of PEGylated NPs. As uncovered in the experiments, the cellular uptake efficiency of PEGylated NP, proportional to its internalization rate, heavily depends on the size of the core and grafting (ligand) density of PEG polymers [28,30,32,33]. To evaluate the cellular uptake efficiency from our DPD simulation results, we take the wrapping time τ_w, i.e. the time to be fully wrapped by the membrane, for the PEGylated NP with $\sigma_p = 1.0$ chains/nm^2 as a baseline. The cellular uptake of the PEGylated NPs can be calculated as $\tau_w/\tau_w(\sigma_p)$, where $\tau_w(\sigma_p)$ is the time for a PEGylated NP at grafting density σ_p to be fully internalized (wrapping ratio unity). If the PEGylated NP cannot be fully internalized (long-lived partial wrapping), we take the wrapping time $\tau_w(\sigma_p) = \infty$. The cellular uptake of PEGylated NPs with different grafting densities is given in Fig. 9a with ligand-receptor binding strength 6.2 k_BT. As we have observed in Fig. 3, when σ_p is small, the cellular uptake efficiency is small as well. The efficiency rapidly increases and saturates at high σ_p~0.8 chains/nm^2 where the cellular uptake efficiency exceeds 80%. Walkey et al. have studied the serum-independent J774A.1 uptake of PEGylated Au NPs in serum-free media [33]. They suggest that uptake results from direct interactions between the distal methoxy group at the free ends of the PEG chains and the membrane surface proteins or lipids [33,49]. These interactions can be weaker hydrophobic interactions or hydrogen bonding [33,49], with binding strength ranging from 2 to 7 k_BT [62]. Therefore, these methoxy groups at free ends of PEG polymers essentially act as 'weak' and 'non-specific' targeting moieties by interacting with cell-surface biomolecules. A similar mechanism is at play in our case. The J774A.1 uptake of PEGylated Au NPs is also given in Fig. 9a for comparison with our simulation results. Interestingly, we find the cellular uptake predicted by our DPD simulations to agree reasonably well with their experimental measurements, although the core diameter of PEGylated Au NPs is about 15 nm with grafted PEG with $N = 112$ monomers [33]. Above $\sigma_p = 0.8$ chains/nm^2, they also find the cellular uptake to completely saturate. The qualitative agreement between our simulation results and the experimental observations on the cellular uptake further verify and validate our model and methodology. More importantly, the optimal σ_p~0.8 chains/nm^2, predicted by the DPD simulations is in agreement with the experimental results. Representative TEM images for J774A.1 uptake of PEGylated Au NPs with grafting density 0.96 chains/nm^2 are displayed in Fig. 9b. At this high grafting density, most of the PEGylated NPs are taken up by the cell, in contrast to the PEGylated NPs with 0.2 chains/nm^2 distributed at the cellular periphery (Fig. 3). Moreover, these PEGylated NPs are mostly dispersed at low density in the cytoplasm.

As shown in the phase diagram (Fig. 6), an optimal $\sigma_p = 0.8$ chains/nm^2 corresponds to the density at which the critical binding strength ε_b levels off. From the cellular uptake efficiency estimated in Fig. 9, such an optimal σ_p also allows efficient internalization of PEGylated NPs. Experimentally, at this grafting density the adsorption of serum protein of PEGylated Au NPs has been tremendously reduced, and the corresponding non-specific macrophage uptake is dramatically decreased [30,33]. Therefore, the optimal σ_p~0.8 chains/nm^2, not only balances F_{ligand} with F_{memb} and $F_{polymer}$, but also reduces the opsonization at the same time.

The current model also has certain limitations. As it has been discussed in the previous work [17], the computational models usually use very high ligand and receptor densities to accelerate simulations [15,20,21,42,58,63], owing to the extremely high computational costs. Therefore, the internalization rate of the NPs from simulations is typically much faster than that observed from experiments [7,64]. Besides, the specific ligand-receptor interactions are simplified as attractive interactions to further reduce the computational costs [15,20,21,42,58,63], which may alter the entropy and free energy of the binding due to the flexure of receptors [54,55,65]. However, the endocytic kinetics can also be quantitatively captured by these accelerated simulations, for NPs with different sizes, shapes and ligand densities [2,15,16,20,22,35,37,39,40,43,57]. Thus, the simulation results given by the present study still provide the detailed understandings on the internalization behaviors of PEGylated NPs.

Both grafting (ligand) density σ_p and degree of polymerization N of grafted PEG are found to play important roles during cellular

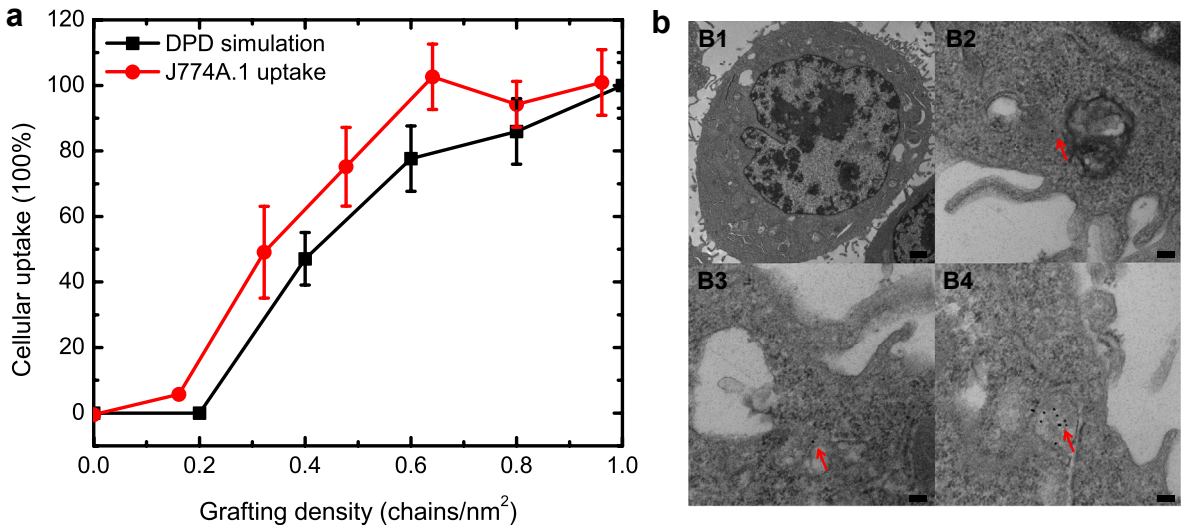

Fig. 9. Effect of grafting density on the cellular uptake efficiency, which is proportional to the internalization rate of PEGylated NPs. The core diameter of PEGylated NPs is 8 nm with grafted PEG of $N = 18$. The ligand-receptor binding strength is $\varepsilon_b = 6.2k_BT$. In (a), Experimental results by Walkey et al. [33] for J774A.1 uptake of PEGylated Au NPs are shown for comparison with our DPD results. (b) Representative TEM images on the intracellular distribution of PEGylated Au NPs with grafting density 0.96 chains/nm^2 and core diameter 15 nm (B1:scale bar = 1000 nm. B2–B4: scale bar = 100 nm). Images B1–B4 are reproduced with permission from Walkey et al. [33].

uptake. Especially, the effect of N on the time scale of internalization and free energy barrier created by $F_{polymer}$ is very strong, which has not been considered in the previous experimental studies. Due to the high computational demanding for larger values of N, it is a forbidden challenge for the present work to computational study the internalization rates of PEGylated NPs with larger molecular weights. We expect the current simulation results can motivate future experiments to elucidate the critical role played by N.

5. Conclusion

In summary, we have performed large scale DPD simulations on receptor-mediated endocytosis of PEGylated NPs with different grafting densities σ_p and polymerization degrees N. All the free ends of grafted PEG polymers are conjugated with targeting moieties by mimicking the experimental conditions, which can specifically recognize and bind to receptors expressed over the cell membrane. The PEGylated NPs with high grafting (ligand) densities can be more easily wrapped by a zero-tension and receptor rich (50%) lipid bilayer, driven by the ligand-receptor binding energy, than PEGylated NPs with low grafting (ligand) densities. The non-specific steric repulsion, $F_{polymer}$, induced by the PEG polymers confined by the membrane, is found to be comparable, or even larger than, the bending energy of the membrane F_{memb} during endocytosis based on our SCF calculations. Therefore, for internalization to occur, the ligand-receptor binding energy, F_{ligand}, must be large enough to overcome the energy barriers created by F_{memb} and $F_{polymer}$. The critical ligand-receptor binding strength for PEGylated NPs to be fully wrapped can be correctly predicted by a simple analytical equation, by including the contribution from $F_{polymer}$. Under a fixed core diameter (8 nm) and polymerization degree of the grafted PEG chains ($N = 18$), an optimal grafting density $\sigma_p \sim 0.8$ chains/nm^2 is identified, which balances F_{ligand} with F_{memb} and $F_{polymer}$, and enables the PEGylated NP to be quickly accepted by the cell. At the same time, this optimal σ_p prevents the absorption of serum-protein and reduces the non-specific uptake of PEGylated NPs by macrophages. For grafted PEG polymers with larger $N = 36$, the overall size of the PEGylated NPs is larger as well, leading to a reduced internalization rate. $F_{polymer}$ for $N = 36$ is also found to be 2–3 times larger than that of $N = 18$, indicating that $F_{polymer}$ can play the dominant role during the endocytosis of PEGylated NPs with long grafted PEG chains. These findings are of immediate interests to the study of cellular uptake of PEGylated NPs and can be further utilized in the design of PEGylated NPs in nanomedicine.

Acknowledgment

The support of this research by National Science Foundation (NSF) is gratefully acknowledged. We are grateful to Wylie Stroberg, Jacob Smith, and Brendan Abberton for critical reading of the manuscript and helpful discussions. Y.L. warmly thanks the financial support provided by Ryan Fellowship and Royal E. Cabell Terminal Year Fellowship at Northwestern University, and helpful discussions with Liangliang Hao. W.K.L. is an Adjunct Professor under the Distinguished Scientists Program Committee at King Abdulaziz University (KAU), Jeddah, Saudi Arabia. This research used resources including the QUEST cluster at NWU and the Argonne Leadership Computing Facility at Argonne Natl. Lab. (supported by the Office of Science of the U.S. Department of Energy under contract DE-AC02-06CH11357).

Appendix A. Supplementary data

Supplementary data related to this article can be found at http://dx.doi.org/10.1016/j.biomaterials.2014.06.032.

References

[1] Alivisatos P. The use of nanocrystals in biological detection. Nat Biotechnol 2004;22:47–52.
[2] Zhang LF, Chan JM, Gu FX, Rhee JW, Wang AZ, Radovic-Moreno AF, et al. Self-assembled lipid-polymer hybrid nanoparticles: a robust drug delivery platform. ACS Nano 2008;2:1696–702.
[3] Doherty GJ, McMahon HT. Mechanisms of endocytosis. Annu Rev Biochem 2009;78:857–902.
[4] Chou LYT, Ming K, Chan WCW. Strategies for the intracellular delivery of nanoparticles. Chem Soc Rev 2011;40:233–45.
[5] Yan Y, Such GK, Johnston APR, Best JP, Caruso F. Engineering particles for therapeutic delivery: prospects and challenges. ACS Nano 2012;6:3663–9.
[6] Canton I, Battaglia G. Endocytosis at the nanoscale. Chem Soc Rev 2012;41:2718–39.

[7] Li Y, Stroberg W, Lee TR, Kim HS, Man H, Ho D, et al. Multiscale modeling and uncertainty quantification in nanoparticle-mediated drug/gene delivery. Comput Mech 2014;53:511–37.
[8] Gao HJ, Shi WD, Freund LB. Mechanics of receptor-mediated endocytosis. P Natl Acad Sci U S A 2005;102:9469–74.
[9] Zhang SL, Li J, Lykotrafitis G, Bao G, Suresh S. Size-dependent endocytosis of nanoparticles. Adv Mater 2009;21:419–24.
[10] Decuzzi P, Ferrari M. The role of specific and non-specific interactions in receptor-mediated endocytosis of nanoparticles. Biomaterials 2007;28:2915–22.
[11] Aoyama Y, Kanamori T, Nakai T, Sasaki T, Horiuchi S, Sando S, et al. Artificial viruses and their application to gene delivery. size-controlled gene coating with glycocluster nanoparticles. J Am Chem Soc 2003;125:3455–7.
[12] Jiang W, Kim BYS, Rutka JT, Chan WCW. Nanoparticle-mediated cellular response is size-dependent. Nat Nanotechnol 2008;3:145–50.
[13] Yuan HY, Li J, Bao G, Zhang SL. Variable nanoparticle-cell adhesion strength regulates cellular uptake. Phys Rev Lett 2010;105:138101.
[14] Decuzzi P, Ferrari M. Design maps for nanoparticles targeting the diseased microvasculature. Biomaterials 2008;29:377–84.
[15] Vacha R, Martinez-Veracoechea FJ, Frenkel D. Receptor-mediated endocytosis of nanoparticles of various shapes. Nano Lett 2011;11:5391–5.
[16] Yue TT, Zhang XR. Cooperative effect in receptor-mediated endocytosis of multiple nanoparticles. ACS Nano 2012;6:3196–205.
[17] Huang CJ, Zhang Y, Yuan HY, Gao HJ, Zhang SL. Role of nanoparticle geometry in endocytosis: laying down to stand up. Nano Lett 2013;13:4546–50.
[18] Decuzzi P, Ferrari M. The receptor-mediated endocytosis of nonspherical particles. Biophys J 2008;94:3790–7.
[19] Cho EC, Zhang Q, Xia YN. The effect of sedimentation and diffusion on cellular uptake of gold nanoparticles. Nat Nanotechnol 2011;6:385–91.
[20] Yang K, Ma YQ. Computer simulation of the translocation of nanoparticles with different shapes across a lipid bilayer. Nat Nanotechnol 2010;5:579–83.
[21] Ding HM, Tian WD, Ma YQ. Designing nanoparticle translocation through membranes by computer simulations. ACS Nano 2012;6:1230–8.
[22] Li YF, Yuan HY, von dem Bussche A, Creighton M, Hurt RH, Kane AB, et al. Graphene microsheets enter cells through spontaneous membrane penetration at edge asperities and corner sites. P Natl Acad Sci U S A 2013;110:12295–300.
[23] Dellian M, Yuan F, Trubetskoy VS, Torchilin VP, Jain RK. Vascular permeability in a human tumour xenograft: molecular charge dependence. Br J Cancer 2000;82:1513–8.
[24] De Jong WH, Hagens WI, Krystek P, Burger MC, Sips AJAM, Geertsma RE. Particle size-dependent organ distribution of gold nanoparticles after intravenous administration. Biomaterials 2008;29:1912–9.
[25] Immordino ML, Dosio F, Cattel L. Stealth liposomes: review of the basic science, rationale, and clinical applications, existing and potential. Int J Nanomed 2006;1:297–315.
[26] Nativo P, Prior IA, Brust M. Uptake and intracellular fate of surface-modified gold nanoparticles. ACS Nano 2008;2:1639–44.
[27] Tkachenko AG, Xie H, Coleman D, Glomm W, Ryan J, Anderson MF, et al. Multifunctional gold nanoparticle-peptide complexes for nuclear targeting. J Am Chem Soc 2003;125:4700–1.
[28] Oh E, Delehanty JB, Sapsford KE, Susumu K, Goswami R, Blanco-Canosa JB, et al. Cellular uptake and fate of PEGylated gold nanoparticles is dependent on both cell-penetration peptides and particle size. ACS Nano 2011;5:6434–48.
[29] de la Zerda A, Bodapati S, Teed R, May SY, Tabakman SM, Liu Z, et al. Family of enhanced photoacoustic imaging agents for high-sensitivity and multiplexing studies in living mice. ACS Nano 2012;6:4694–701.
[30] Chen HW, Paholak H, Ito M, Sansanaphongpricha K, Qian W, Che Y, et al. 'Living' PEGylation on gold nanoparticles to optimize cancer cell uptake by controlling targeting ligand and charge densities. Nanotechnology 2013;24:355101.
[31] Arnida, Malugin A, Ghandehari H. Cellular uptake and toxicity of gold nanoparticles in prostate cancer cells: a comparative study of rods and spheres. J Appl Toxicol 2010;30:212–7.
[32] Cho EC, Au L, Zhang Q, Xia YN. The effects of size, shape, and surface functional group of gold nanostructures on their adsorption and internalization by cells. Small 2010;6:517–22.
[33] Walkey CD, Olsen JB, Guo HB, Emili A, Chan WCW. Nanoparticle size and surface chemistry determine serum protein adsorption and macrophage uptake. J Am Chem Soc 2012;134:2139–47.
[34] Groot RD, Rabone KL. Mesoscopic simulation of cell membrane damage, morphology change and rupture by nonionic surfactants. Biophys J 2001;81:725–36.
[35] Li YF, Li XJ, Li ZH, Gao HJ. Surface-structure-regulated penetration of nanoparticles across a cell membrane. Nanoscale 2012;4:3768–75.
[36] Mao J, Guo R, Yan LT. Simulation and analysis of cellular internalization pathways and membrane perturbation for graphene nanosheets. Biomaterials 2014;35:6069–77.
[37] Guo RH, Mao J, Yan LT. Unique dynamical approach of fully wrapping dendrimer-like soft nanoparticles by lipid bilayer membrane. ACS Nano 2013;7:10646–53.
[38] Hong BB, Qiu F, Zhang HD, Yang YL. Budding dynamics of individual domains in multicomponent membranes simulated by N-varied dissipative particle dynamics. J Phys Chem B 2007;111:5837–49.
[39] Yue TT, Zhang XR. Molecular modeling of the pathways of vesicle-membrane interaction. Soft Matter 2013;9:559–69.
[40] Yue TT, Zhang XR, Huang F. Membrane monolayer protrusion mediates a new nanoparticle wrapping pathway. Soft Matter 2014;10:2024–34.
[41] Lee H, de Vries AH, Marrink SJ, Pastor RW. A coarse-grained model for polyethylene oxide and polyethylene glycol: conformation and hydrodynamics. J Phys Chem B 2009;113:13186–94.
[42] Ding HM, Ma YQ. Controlling cellular uptake of nanoparticles with pH-sensitive polymers. Sci Rep 2013;3:2804.
[43] Li Y, Yue TT, Yang K, Zhang XR. Molecular modeling of the relationship between nanoparticle shape anisotropy and endocytosis kinetics. Biomaterials 2012;33:4965–73.
[44] Halperin A, Kröger M, Zhulina EB. Colloid-brush interactions: the effect of solvent quality. Macromolecules 2011;44:3622–38.
[45] Wijmans CM, Zhulina EB. Polymer brushes at curved surfaces. Macromolecules 1993;26:7214–24.
[46] Scheutjens JMHM, Fleer GJ. Statistical-theory of the adsorption of interacting chain molecules. 1. partition-function, segment density distribution, and adsorption-isotherms. J Phys Chem 1979;83:1619–35.
[47] Szleifer I, Carignano MA. Tethered polymer layers: phase transitions and reduction of protein adsorption. Macromol Rapid Comm 2000;21:423–48.
[48] Szleifer I. Protein adsorption on surfaces with grafted polymers: a theoretical approach. Biophys J 1997;72:595–612.
[49] Unsworth LD, Sheardown H, Brash JL. Protein-resistant poly(ethylene oxide)-grafted surfaces: chain density-dependent multiple mechanisms of action. Langmuir 2008;24:1924–9.
[50] Kröger M, Peleg O, Halperin A. From dendrimers to dendronized polymers and forests: scaling theory and its limitations. Macromolecules 2010;43:6213–24.
[51] Chen XM, Tian FL, Zhang XR, Wang WC. Internalization pathways of nanoparticles and their interaction with a vesicle. Soft Matter 2013;9:7592–600.
[52] Footer MJ, Kerssemakers JWJ, Theriot JA, Dogterom M. Direct measurement of force generation by actin filament polymerization using an optical trap. P Natl Acad Sci U S A 2007;104:2181–6.
[53] Galletta BJ, Cooper JA. Actin and endocytosis: mechanisms and phylogeny. Curr Opin Cell Biol 2009;21:20–7.
[54] Liu J, Weller GER, Zern B, Ayyaswamy PS, Eckmann DM, Muzykantov VR, et al. Computational model for nanocarrier binding to endothelium validated using in vivo, in vitro, and atomic force microscopy experiments. P Natl Acad Sci U S A 2010;107:16530–5.
[55] Bradley R, Radhakrishnan R. Coarse-grained models for protein-cell membrane interactions. Polymers 2013;5:890–936.
[56] Deserno M, Gelbart WM. Adhesion and wrapping in colloid-vesicle complexes. J Phys Chem B 2002;106:5543–52.
[57] Ruiz-Herrero T, Velasco E, Hagan MF. Mechanisms of budding of nanoscale particles through lipid bilayers. J Phys Chem B 2012;116:9595–603.
[58] Yi X, Shi XH, Gao HJ. A universal law for cell uptake of one-dimensional nanomaterials. Nano Lett 2014;14:1049–55.
[59] Byfield FJ, Aranda-Espinoza H, Romanenko VG, Rothblat GH, Levitan I. Cholesterol depletion increases membrane stiffness of aortic endothelial cells. Biophys J 2004;87:3336–43.
[60] Halperin A, Kröger M. Theoretical considerations on mechanisms of harvesting cells cultured on thermoresponsive polymer brushes. Biomaterials 2012;33:4975–87.
[61] Halperin A, Kröger M. Thermoresponsive cell culture substrates based on PNIPAM brushes functionalized with adhesion peptides: theoretical considerations of mechanism and design. Langmuir 2012;28:16623–37.
[62] Markovitch O, Agmon N. Structure and energetics of the hydronium hydration shells. J Phys Chem A 2007;111:2253–6.
[63] Shi XH, von dem Bussche A, Hurt RH, Kane AB, Gao HJ. Cell entry of one-dimensional nanomaterials occurs by tip recognition and rotation. Nat Nanotechnol 2011;6:714–9.
[64] van de Ven AL, Kim P, Haley O, Fakhoury JR, Adriani G, Schmulen J, et al. Rapid tumoritropic accumulation of systemically injected plateloid particles and their biodistribution. J Control Release 2012;158:148–55.
[65] Liu J, Bradley R, Eckmann DM, Ayyaswamy PS, Radhakrishnan R. Multiscale modeling of functionalized nanocarriers in targeted drug delivery. Curr Nanosci 2011;7:727–35.